# Evaluating pixel and object based image classification techniques for mapping plant invasions from UAV derived aerial imagery: *Harrisia pomanensis* as a case study

**Madodomzi Mafanya [1,3,4]*, Philemon Tsele [1], Joel Botai [2], Phetole Manyama [3], Barend Swart [4] and Thabang Monate [4]**

[1] Department of Geography, Geoinformatics and Meteorology, University of Pretoria, Pretoria, South Africa; E-mail: muzianho@gmail.com ; philemon.tsele@up.ac.za

[2] South African Weather Services, Pretoria, South Africa; E-mail: joel.botai@weathersa.co.za

[3] South African National Biodiversity Institute, Invasive Species Programme, Pretoria, South Africa; E-mail : p.manyama@sanbi.org.za ; invasivespecies@sanbi.org.za

[4] CAD Mapping Aerial Surveyors, Pretoria, South Africa; E-mail : barend@cadmapping.co.za, tjmonate@gmail.com

* Correspondence; E-mail: muzianho@gmail.com; Tel.: +27-769-090-497

**Abstract:** Invasive alien plants (IAPs) not only pose a serious threat to biodiversity and water resources but also have impacts on human and animal wellbeing. To support decision making in IAPs monitoring, semi-automated image classifiers which are capable of extracting valuable information in remotely sensed data are vital. This study evaluated the mapping accuracies of supervised and unsupervised image classifiers for mapping *Harrisia pomanensis* (a cactus plant commonly known as the Midnight Lady) using two interlinked evaluation strategies i.e. point and area based accuracy assessment. Results of the point-based accuracy assessment show that with reference to 219 ground control points, the supervised image classifiers (i.e. *Maxver* and *Bhattacharya*) mapped *H. pomanensis* better than the unsupervised image classifiers (i.e. *K-mediuns*, *Euclidian Length* and *Isoseg*). In this regard, user and producer accuracies were 82.4 % and 84% respectively for the *Maxver* classifier. The user and producer accuracies for the *Bhattacharya* classifier were 90% and 95.7%, respectively. Though the *Maxver* produced a higher overall accuracy and Kappa estimate than the *Bhattacharya* classifier, the *Maxver* Kappa estimate of 0.8305 is not significantly (statistically) greater than the *Bhattacharya* Kappa estimate of 0.8088 at a 95% confidence interval. The area based accuracy assessment results show that the *Bhattacharya* classifier estimated the spatial extent of *H. pomanensis* with an average mapping accuracy of 86.1% whereas the *Maxver* classifier only gave an average mapping accuracy of 65.2%. Based on these results, the *Bhattacharya* classifier is therefore recommended for mapping *H. pomanensis*. These findings will aid in the algorithm choice making for the development of a semi-automated image classification system for mapping IAPs.

**Key Words:** Pixel- and object-based classification; Invasive Alien plants; UAV; *Harrisia pomanensis*; Point- and area-based accuracy assessment.

## 1. Introduction

Invasive alien plants (IAPs) not only pose a serious threat to biodiversity and water resources but also have impacts on human and animal wellbeing [1]. IAPs alter the functioning of ecosystems by degrading the land, diminishing native flora, reducing farming and grazing potential, and/or by changing soil dynamics and ecosystem fire regimes [2-4]. An important step in IAPs management is to map their location [5-7]. Accurate spatial estimates are crucial because there is a strong correlation between the spatial extent of an invaded area and the effort required for clearing the plant invasion [8]. Spatial data is important in the process of generating simulation models for monitoring control programmes, assessing invasion risk and modelling eradication feasibility [9]. Timely mapping and rapid delimitation of the spatial extent of IAPs can facilitate decision making regarding the feasibility and effectiveness of eradication and/or containment [9]. Remote sensing has the potential to support the use of remotely-sensed observations for locating and managing IAPs [10].

There are two main optical remote sensing approaches for mapping and monitoring IAPs, namely, high spectral resolution with low spatial resolution and high spatial resolution with low spectral resolution [11]. In particular, the high spectral resolution approach entails the use of hyperspectral sensors for collecting hundreds of narrow bands (less than 10 nm bandwidth) in the visible, near infrared and shortwave infrared regions of the electromagnetic spectrum [12]. For example, Ustin and Santos [13] used field and spaceborne spectroscopy to distinguish between native and non-native plant species based on their spectral signatures. Haung and Asner [12] fused Light Detection and Ranging (LiDAR) data and hyperspectral imagery to delineate the structural and functional properties of IAPs. Further, Williams and Hunt [14] reported a 95% overall accuracy for mapping leafy spurge (*Euphorbia esula* L.) using the Airborne Visible/Infrared Spectrometer (AVIRIS) hyperspectral data. Notwithstanding these successful attempts, currently, using hyperspectral data in mapping IAPs has several limitations such as the high cost of satellite hyperspectral data, airborne and handheld sensors as well as the resultant large volumes of data that require high computing power for processing [15].

The high spatial resolution approach usually makes use of spaceborne and/or airborne multispectral imagery as well as aerial photography. For instance, Ngubane et al. [16] obtained 79.14%, 97.62% and 91.11% for the overall, user and producer accuracies, respectively, by using World-View 2 imagery at 2m spatial resolution for mapping the invasive brackern fern in the KwaZulu Natal Province of South Africa. Even though canopy dominating IAPs as well as IAPs that are phenologically different from background vegetation can be mapped using spaceborne multispectral imagery, this technique performs poorly for mapping understorey IAPs [9]. Moreover, low spectral resolution limits the application of multi-spectral satellite imagery in species specific monitoring of IAPs especially when the species of concern is phenologically invariant from its background vegetation [17].

Moreover, Müllerová et al. [18] used time series analysis to measure the spatial extent and the rate of areal spread of the *Heracleum mantegazzianum* (giant hogweed) in the Czech Republic using colour aerial photography. However, airborne multispectral sensors on board manned aircrafts may give inadequate spatial resolution for species specific detection of IAPs [19]. To address the problem of data acquisition costs and the insufficient spatial resolution in multispectral data and traditional aerial photography, use of Unmanned Aerial Vehicles (UAVs) can be made as this option allows for rapid acquisition of low cost ultra-high spatial resolution imagery [20].

The developments in UAV technology have afforded the remote sensing community the opportunity to map the environment at enhanced spatial resolutions. Use of consumer grade digital cameras with very high spatial but low spectral resolution in UAV remote sensing is often used due to the limited payload capacity on these systems (<50 kg) [21]. For example, in the Czech Republic, Dvořák et al. [22] developed a rapid, repeatable and efficient UAV based method for the mapping and monitoring of IAPs from consumer grade digital cameras. Use of UAVs for producing high spatial resolution datasets has several advantages over the manned aircraft or spaceborne platforms for accurately mapping IAPs and these include flexible temporal resolution and low data acquisition costs [22]. The high spatial resolution can be attributed to the fact that UAV systems allow for data acquisition at low flight altitudes of usually less than 150m above ground level. The effect of high spatial resolution was demonstrated in [23] whereby a 94% overall accuracy for mapping IAPs was obtained using 80 cm UAV-derived imagery. Furthermore, frequent IAPs monitoring efforts based on remotely sensed imagery may require development of semi-automatic image classification systems that are able to map, quantify and monitor the presence of IAPs in remotely sensed data [17]. Supervised or unsupervised (pixel, object based and hybrid) classification approaches are tested for mapping IAPs [22]. In particular, iterative semi-automated object based classification approaches are tested for mapping IAPs such as *Heracleum mantegazzianum (*giant hogweed) from high spatial resolution UAV-derived data [24]. For very high resolution imagery, the object-based image classification techniques have demonstrated improved performances over the pixel based approach [25]. The first and critical step in object-based image classification is segmentation which encompasses grouping of similar pixels, according to some similarity threshold, into homogenous objects [26, 27]. Therefore, the object-based image analysis (OBIA) techniques do not only allow for the consideration of spectral information but also contextual, textural, shape and spatial relationships in image objects as opposed to single pixels [26, 28, and 29]. The objective of the current study is to evaluate pixel and object based image classifiers for mapping *Harrisia pomanensis* (The Midnight Lady), a particular plant invasion from ultra-high spatial resolution (5cm) UAV derived imagery. The results of this evaluation shall then be used to guide the decision as to which image classifiers to be used when developing a semi-automated image classification system for mapping the target plant.

This study compared five image classifiers using two different interlinked evaluation strategies. The evaluation strategies used are point and area based accuracy assessment. The compared classifiers were unsupervised pixel based classifiers (*k-mediuns* and *Euclidian Length*), unsupervised object based classifier (*Isoseg*), supervised pixel based classifier (*Maxver*) and supervised object based classifier (*Bhattacharya*). The image classification for this study was done in the Spring open source software [30]. The objective of this research is to contribute towards the development of a semi-automated image classification system for mapping IAPs.

## 2. Description of the study area, species and data-sets used.

### *2.1. Study area*

The study area is located near the Alldays town within Waterberg district municipality of the Limpopo province of South Africa (Figure 1a). The area is characterised by a semi-arid climate and falls within the summer rainfall region which experiences average midday temperatures of 22.3 °C and 31.9 °C in winter (June to August) and summer (October to February) seasons, respectively [31]. The rainfall amount is estimated at 0 mm in winter and could escalate to a maximum of approximately 81 mm in summer [31]. Furthermore, the 872 000 $m^2$ spatial extent study area (Figure 1b) is a flat terrain woodland with orthometric height values ranging from 800 m to 817m.

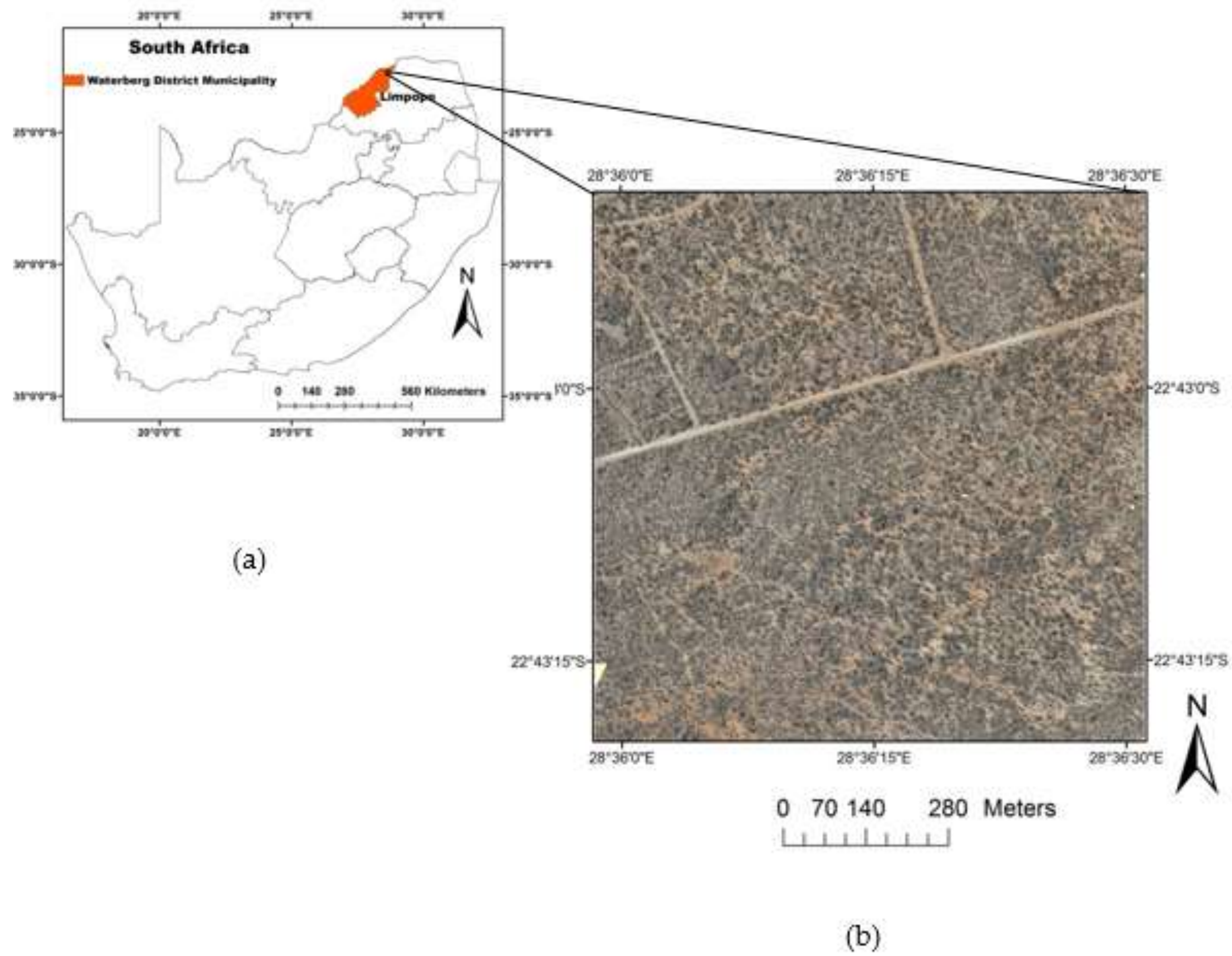


**Figure 1**. a) Map of South Africa showing the location of Waterberg district municipality within the Limpopo province. The RGB image shown in b) is the actual UAV derived 872 000m$^2$ orthomosaic of the study area based upon which image classification was performed.

*2.2. Species description and mapping methods*

*Harrisia pomanensis*, commonly known as the Midnight lady is a succulent cactus that belongs to the Harrisia genus (Figure 2). *H. pomanensis* plants have jointed spiny fleshy stems with thorny spikes and when these stems touch the ground, they develop roots and spread. *H. pomanensis* was detected by the South African National Biodiversity Institute: Invasive Species Programme (SANBI ISP) in 2011 as part of on-going efforts at incursion response planning [8]. This plant colonises farms making it hard for farmers to use the land for cropping, block the mobility of livestock, injure animals and reduce grazing land. This plant invasion has been spotted by SANBI ISP field teams in a farming area of not less than 100 000 000 m$^2$. Other tree species in the invaded woodland include *Commiphora mollis* (velvet-leaved corkwood), *Commiphora neglecta*

(Green-temmed corkwood), *Acacia robusta* (Broad pod robust thorn), *Acacia mellifera* (Black thorn), *Kirkia acuminata (*White seringa), *Lannea sp.* (False marulas) and *Sclerocarya birrea* (Marula) etc. Handheld GPS based field campaigns for mapping *H. pomanensis* pose a human risk due to the dense cluster nature of the woodland and the availability of thorns and dangerous animals. The UAV based Remote Sensing approach allows for mapping of areas larger than 2 000 000m$^2$ per flight while enabling detection of small plant invasion clumps that could have been missed by field teams, again due to the densely-clustered nature of the woodland. Thus this approach allows for timely, efficient and less laborious mapping when compared to handheld GPS based surveying of the target plant. For image classification purposes, four land cover types were identified on the field (i.e. ground, coniferous trees, deciduous trees and *H. pomanensis*).

**Figure 2:** Depiction of the *Harrisia pomanensis* invasive plant in the winter season near Alldays town in the Limpopo province, South Africa

2.3. *Data-sets used*

2.3.1. Ground Control Points

In this study, ground control points (GCPs) were recorded using the Global Navigation Satellite System - Real Time Kinematic (GNSS-RTK) method. The GNSS-RTK method uses a network of widely spaced continuously operating base stations to give a positional correction to a user rover and a RTK network usually has at least one central processing station [32]. The RTK network used in this study was the South African network of TrigNet base stations whose central processing station is located at the South African Chief Directorate: National Geospatial Information offices in Mowbray, Cape Town [33]. JAVAD Triumph-1M, a high precision 864 channel chip GNSS receiver was used for capturing the topographic GCP points. The International Terrestrial Reference Frame 2008 (ITRF2008) ellipsoidal height values were converted to orthometric heights by applying the South African GEOID 2010 separation model which is a closer approximation to the height above sea level [34]. Moreover, a horizontal shift from ITRF2008 WGS84 to the South African Hartesbeesthoek 1994 datum was applied.

Two sets of GCPs were logged, namely, orthorectification points and accuracy assessment reference points. For the orthorectification points, yellow markers were placed on the ground and surveyed for accurate georeferencing of the UAV derived orthomosaic as done in [20]. The orthorectification data-set was used for georeferencing the UAV RGB image during image mosaicking as applied in [35]. Additionally, a set of GNSS-RTK accuracy assessment reference points ($N_1$=119) were surveyed using the stratified random sampling method. This method was used primarily due to the uneven spatial distribution of the four land cover classes under consideration in this study. For instance, across the scene there was more exposed ground than vegetation (i.e. deciduous trees, coniferous trees and *H. pomanensis*). Thus the stratification ensured representative distribution of the GCPs across all four land cover classes through the selection of primary sampling units (PSUs) [36]. In each PSU, points for all four land cover classes were surveyed randomly using the GNSS-RTK method. In addition to the GNSS-RTK derived accuracy assessment reference points, another set of independently-derived random points ($N_2$ =100) was generated in ArcGIS ArcMap 10.4 [37], so as to introduce randomness and statistical soundness in the reference points data-set.

2.3.2. UAV flight planning and image pre-processing

Both co-located GCPs and the UAV imagery were captured on the 13th of August, 2015.The Ardupilot open source Mission Planner [38] was used for flight planning and real time flight management. An over the counter RGB Canon S110 camera with a spectral range of approximately 390nm-710nm was mounted onto the UAV which was flown at 100m altitude above ground level to produce imagery with 3.65 cm spatial resolution. Each raw image had a ground side width of 146.2 m and a forward swath of 109.6 m. The UAV system had a total mass of 3.6 kg and were flown at a ground speed of around 60 km per hour. Further, the GNSS/INS system on-board the UAV was logging GPS co-ordinates of each captured image as events which were later used to geotag the raw images using Mission Planner. The side overlap for neighbouring images was set to 60% while the forward overlap was set to 80%. This image sampling redundancy is critical for generating 3D point clouds, digital surface models (DSMs), and orthomosaic using Unmanned Aerial Vehicles –Structure from Motion (UAV-SfM). The proprietary Agisoft Photoscan [39] software package was used for image mosaicking using UAV-SfM in this study. Structure from Motion (SfM) is a photogrammetric 3D reconstruction technique that uses overlapping 2D images to create 3D point clouds, DSMs and orthomosaic. SfM involves three stages of feature detection, image matching and bundle block adjustment [40].The geotagged raw images were administered into this photogrammetry software package together with GCPs to produce the georectified RGB orthomosaic used for image classification (Figure 1b).

## 3. Analysis methods

### *3.1. Description of the selected image classifiers*

Five image classifiers of both pixel and object based were evaluated in order to determine the classifier with the lowest omission and commission errors for mapping *H. pomanensis* from the UAV imagery. The considered image classifiers were the unsupervised pixel based (*K-mediuns* and *Euclidian length*), unsupervised object based (*Isoseg*), supervised pixel based (*Maxver*) and the supervised object based image classifier (*Bhattacharya*) [30]. The *k-mediuns* classifier considers the median vector of a pixel and assigns the pixel to a class with the closest class median vector according to a similarity threshold. This is a good comparison because the median is known to be less sensitive to outliers than the mean. On the other hand, the *Euclidian length* classifier uses an algorithm that calculates the Euclidean distance between a pixel spectral mean vector and a class mean vector and then assign the pixel to the class of shortest distance according to a similarity threshold [41]. In this study, both of these classifiers were used to generate 16 unsupervised classes that were later grouped into four the land cover classes (ground, conifers, deciduous trees and *H. pomanensis*).

The *Maxver* classifier uses the Maximum Likelihood (ML) algorithm which assumes that the digital numbers of a class in the image bands are normally distributed and calculates the probability of each pixel belonging to that class [42]. ML takes into account the mean and covariance vectors of the training sets of a class in a 3-dimensional space and assigns each pixel to the class for which it has the highest probability of membership [43]. Since the *Maxver* classifier is a supervised classification technique, all pixels were assigned to the four land cover classes. The classes were created during the training stage of image classification.

While the pixel based image classifiers described above assign pixels to classes, the object based image classifiers (e.g. *Isoseg* and *Bhattacharya*) classify objects or segments instead of pixels. This means that image segmentation is the first step in object based image classification and partitions the image into objects by grouping associated pixels together using a similarity threshold. The partitioning of the remotely sensed image into segments is important because images contain spatial and textural information which is neglected in pixel based image classification techniques [44]. In this study, the UAV orthomosaic was segmented using the *region growing* technique. After some trial runs, a grouping of 350 pixels with 6 similarities was found to be good parameters for partitioning the UAV derived RGB orthomosaic used in this study as this grouping provided large enough but non class mixing objects.

The *Isoseg* classifier assigns segments to a class using the Mahalanobis distance which is the dissimilarity measure between a segment mean vector *x* and a class mean vector *y* of the same probability distribution with covariance [45]. The *Isoseg* classifier makes use of the K-means algorithm to decide whether a particular segment belongs to a certain class. A 3 dimensional decision surface, which is a hyperellipsoid, is created for each class and this surface has a mean vector (i.e. the mean vector of the class). The K-means algorithm uses the mean vector of the class in question as an initial centre and then all segments whose means fall inside this class's hyperellipsoid are assigned to that particular class because such segments meet the criteria according to the analyst specified Chi-square acceptable threshold percentage [46]. Similar classes are then merged together [47]. The 16 generated classes were then merged into the four land cover classes under consideration in this study.

The *Bhattacharya* classifier on the other hand uses the Bhattacharya distance which measures the similarity of probability distribution curves between a candidate segment and a class [48]. The Bhattacharya distance is the distance between the centres (i.e. means) of those two probability distributions. Segments that are closely inside a particular class's distribution threshold compared to other classes are assigned to that particular class [30]. Since the *Bhattacharya* classifier is a supervised image classification technique, all segments were assigned to the predefined four land cover classes. The classes were created during the training stage of image classification.

*3.2.Accuracy assessment*

3.2.1. Point based accuracy assessment

For each of the 5 classifiers, 3 error matrices were generated based on the (i) GNSS-RTK points ($N_1$=119), (ii) independently-derived random points (($N_2$=100) and (iii) combined set of reference points ($N_3$ =219) across the ground, conifers, deciduous trees and *H. pomanensis* land cover types. In addition, the overall accuracy and the estimate of Kappa were used to compare classification results of the 5 image classifiers from 15 error matrices across the aforementioned land cover types [49]. Equation 1, 2, 3 and 6 (Table 1) were used to calculate the overall accuracy ($p_o\mathrm{X}$), chance agreement ($p_c\mathrm{X}$), Kappa estimate ($\hat{\mathrm{k}}_{\mathrm{X}}$) and the variance of the Kappa estimate ($\mathrm{var\_}\hat{\mathrm{k}}_{\mathrm{X}}$), respectively. Furthermore, Equation 4 and 5 (Table 1) represent parameters for the computation of the variance $\hat{\mathrm{k}}$ [49].

**Table 1**. Expressions used for calculating the overall accuracy, chance agreement, estimate of Kappa and its variance.

| Equation and statistic name | |
|---|---|
| $p_o\mathrm{X}=\frac{1}{\mathrm{N_X}}.\sum_{i=1}^{n} p_{ii}(\mathrm{X})$ Overall accuracy | (1) |
| $p_c\mathrm{X}=\frac{1}{\mathrm{N^2{}_X}}.\sum_{i=1}^{n}\mathrm{RT}(\mathrm{X})^{<i>}.\mathrm{CT}(\mathrm{X})^{<i>}$ Chance agreement [49] | (2) |
| $\hat{\mathrm{k}}_\mathrm{X}=\frac{p_o\mathrm{X}\text{-}p_c\mathrm{X}}{1-p_c\mathrm{X}}$ Kappa estimate [49] | (3) |
| $\mathrm{a_{1x}}=\sum\left[\frac{1}{\mathrm{N_x}^2}.\sum_{i=1}^{n}\mathrm{X}_{i,i}.(\mathrm{RT_{(X)}}^{<i>}+\mathrm{CT_{(X)}}^{<i>})\right]$ | (4) |
| $\mathrm{a_{2X}}=\sum\left[\frac{1}{\mathrm{N_X}^3}.\sum_{i=1}^{n}\sum_{j=1}^{n}\mathrm{X}_{i,j}.(\mathrm{RT_{(X)}}^{<i>}+\mathrm{CT_{(X)}}^{<j>})^2\right]$ | (5) |
| $\mathrm{var\_}\hat{\mathrm{k}}_\mathrm{X}=\frac{1}{\mathrm{N_X}}.\left[\frac{p_o\mathrm{X}.(1\text{-}p_o\mathrm{X})}{(1-p_c\mathrm{X})^2}+\frac{2.(1-p_o\mathrm{X})(2.p_o\mathrm{X}.p_c\mathrm{X}\text{-}\mathrm{a_{1X}})}{(1-p_c\mathrm{X})^3}+\frac{(1-p_o\mathrm{X})^2.(\mathrm{a_{2X}}-4.p_c\mathrm{X}^2)}{(1-p_c\mathrm{X})^4}\right]$ Variance of the Kappa estimate [49] | (6) |

Where:

$\mathrm{X}$ is the error matrix of either *K-mediuns*, *Euclidian length*, *Isoseg*, *Maxver* or *Bhattacharya* classifier.

$\mathrm{N_X}$ = the total number of reference points

$n$ =4 (i.e. the number of classes viz. Ground, Conifers, Decidous and *H. pomanensis*)

$P_{ii}$ = the number of correct observations for the *i*th class

$\mathrm{RT}(\mathrm{X})^{<i>}$ or $\mathrm{RT_{(X)}}^{<i>}$ = Row Total of the *i*th class

$\mathrm{CT}(\mathrm{X})^{<i>}$ or $\mathrm{CT_{(X)}}^{<j>}$ = Column Total of the *i*th or *j*th class

$p_o\mathrm{X}$ = Overall accuracy

$p_c\mathrm{X}$ = Chance agreement

$\hat{\mathrm{k}}_\mathrm{X}$ = Kappa estimate

$\mathrm{a_{1x}}$ and $\mathrm{a_{2X}}$ are parameters used in the calculation of the variance

$\mathrm{var\_}\hat{\mathrm{k}}_\mathrm{X}$ = Variance of the Kappa estimate [49,50]

3.2.2 Hypothesis testing for point based accuracy assessment

In this study, a statistical hypothesis test was conducted to determine whether the difference between the Kappa values of accuracy assessment results of two classifiers is significantly different [51]. In essence the test was conducted to determine whether the image classifier with the highest Kappa value necessarily produced better classification results than the image classifier with the second highest Kappa value. Given the large sample size (i.e. N<30) of reference data points used in this study for accuracy assessment, the Z- test was applied when conducting the hypothesis test between the Kappa estimates of the two best performing image classifiers [51]. Therefore, the null and alternative hypotheses were formulated as follows;

$$H_0 : \left[ \hat{k}_X - \hat{k}_Y \right] = 0 \tag{7}$$

where $H_0$ denotes the null hypothesis that there is no difference between the classification accuracy results of image classifier X and image classifier Y. $\hat{k}_X$ and $\hat{k}_Y$ denote the Kappa estimates of image classifier X and Y, respectively.

$$H_1 : \left[ \hat{k}_X - \hat{k}_Y \right] > 0 \tag{8}$$

where $H_1$ denotes the alternative hypothesis that the classification accuracy results of image classifier X are significantly greater than those of classifier Y.

Furthermore, the Z-test statistic for determining whether image classifier X produced better classification results than image classifier Y can be calculated as follows [52];

$$Z_{XY} = \frac{\hat{k}_X - \hat{k}_Y}{\sqrt{var\_\hat{k}_X + var\_\hat{k}_Y}} \tag{9}$$

where $Z_{XY}$ is the standard normal deviate. Here we can reject $H_0$ (equation 7) at 95% confidence interval given that $Z_{XY} \geq 1.96$ [52]. However, if $Z_{XY} \leq 1.96$, we cannot reject $H_0$ that the classification results of image classifier X and Y are possibly not different, which means that image classifier X did not produce better classification results than image classifier Y.

3.2.3 Comparison of areal estimates between the *Maxver* and *Bhattacharya* classifiers.

For the area based accuracy assessment, a set of 35 polygons was created through visually interpreting and hand digitising clumps of *H. pomanensis* that varied from 4 $m^2$ to about 60 $m^2$ on the UAV RGB orthomosaic o. During creation of the polygons, care was taken to digitize homogenous pixels that comprise of *H. pomanensis*, while disregarding visible spaces of ground and/or other surrounding land cover types. Thus, the aforementioned polygons were considered as independently-derived reference data for area based accuracy assessment in this study. The polygons were used to compute areal estimates of *H. pomanensis* and compare them to the areal estimates mapped by the *Maxver* and *Bhattacharya* classifiers within those polygons. The polygons were used to assess omission errors. Use of the UAV RGB orthomosaic and thematic maps extracts is made for the qualitative assessment of commission errors in this study.

## 4. Results

*4.1. Point based accuracy assessment using the GNSS-RTK and independently-derived reference data.*

Point based accuracy assessment results of the five image classifiers for mapping *H. pomanensis* are presented in Tables 2-4. In particular, results based on the GNSS-RTK reference points ($N_1$=119) showed that the *Maxver* and *Bhattacharya* classifiers had higher producer accuracies of 83.7% and 95.1% than the unsupervised classifiers, respectively (Table 2). This indicates that the aforementioned supervised classifiers provide better mapping of *H. pomanensis* with low omission errors of 16.3% and 4.9%, respectively. Furthermore, while virtually similar mapping performance with regard to the user accuracies of all classifiers is observed (Table 2), the unsupervised *K-mediuns* classifier had the highest user accuracy that is analogous to 0% commission error. Overall, the *Maxver* and *Bhattacharya* supervised classifiers had the highest overall accuracies of about 90 % with corresponding $\hat{k}$ values of 0.86 and 0.88 respectively.

**Table 2.** Accuracy assessment of the five image classifiers for mapping *Harrisia pomanensis* based on the GNSS-RTK reference points ($N_1$ = 119).

| Classification type: | | Classifier | Producer Accuracy (%) | User Accuracy (%) | Overall Accuracy % | $\hat{k}$ |
|---|---|---|---|---|---|---|
| Unsupervised | Pixel based | *K-mediuns* | 48.8 | 100 | 67.2 | 0.57 |
| | | *Euclidian Length* | 65 | 79 | 75 | 0.66 |
| | Object based | *Isoseg* | 38.8 | 79.2 | 57.1 | 0.41 |
| Supervised | Pixel based | *Maxver* | 83.7 | 87.8 | 89.9 | 0.86 |
| | Object based | *Bhattacharya* | 95.1 | 90.7 | 89.9 | 0.88 |

In addition, other accuracy assessment results based on the set of independently-derived random reference points ($N_2$ =100) are presented in Table 3. A good mapping accuracy of the *Maxver* and *Bhattacharya* supervised classifiers is evident (Table 3) corroborating results in Table 2. In particular, these two classifiers had overall accuracies and kappa values above 0.80 notwithstanding their notable relative performance in the producer and user accuracies, respectively. On the other hand, the unsupervised *Euclidian length* classifier yielded the highest producer accuracy of 94% (compared to all other classifiers) coupled with 75% overall accuracy. Furthermore, the overall accuracies of the *K-mediuns* and *Isoseg* unsupervised classifiers showed an inadequate classification.

**Table 3.** Accuracy assessment of the five classifiers detecting *Harrisia pomanensis* based on the 100 independently-derived reference points.

| Classification type: | | Classifier | Producer Accuracy (%) | User Accuracy (%) | Overall Accuracy (%) | $\hat{k}$ |
|---|---|---|---|---|---|---|
| Unsupervised | Pixel based | *K-mediuns* | 25 | 18.2 | 67 | 0.46 |
| | | *Euclidian Length* | 93.8 | 48.4 | 75 | 0.64 |
| | Object based | *Isoseg* | 12.5 | 14.3 | 64 | 0.36 |
| Supervised | Pixel based | *Maxver* | 75 | 66.7 | 85 | 0.82 |
| | Object based | *Bhattacharya* | 85.7 | 100 | 81.0 | 0.68 |

Furthermore, Table 4 presents another set of accuracy assessment results based on a combined data-set of reference points ($N_3$=219). This set of results gave an indication of consistency in the mapping performance of all five classifiers across all three assessments (Tables 2-4). In particular, the supervised classifiers depict optimal overall accuracy above 80% in all three assessments compared to unsupervised classifiers

(Tables 2-4). Additionally, the results show that the *Maxver* and *Bhattacharya* supervised classifiers can be expected to map *H. pomanensis* with relatively low omission errors of 17.6% and 10% and commission errors of 16% and 4.3%, respectively (Table 4). Such mapping performance was followed by the unsupervised *Euclidian length* classifier with omission error of 27.4% and commission error of 35.7% (Table 4). Thus the best two performing classifiers (*Maxver* and *Bhattacharya*) were further evaluated using error matrices in 4.2 below.

**Table 4.** Accuracy assessment of the five classifiers for detecting *Harrisia pomanensis* based on the 219 reference points.

| ***Harrisia pomanensis* classification accuracy assessment** | | | | **Percent Accuracy** | | | |
|---|---|---|---|---|---|---|---|
| Classification type: | | Classifier | Estimated Area (m$^2$) | Producer | User | Overall | $\hat{k}$ |
| Unsupervised | Pixel based | *K-mediuns* | 77964.8 | 42.3 | 78.6 | 67.1 | 0.49 |
| | | *Euclidian Length* | 249309.2 | 72.6 | 64.3 | 74.9 | 0.66 |
| | Object based | *Isoseg* | 62676.0 | 35.1 | 64.5 | 60.3 | 0.46 |
| Supervised | Pixel based | *Maxver* | 84604.7 | 82.4 | 84 | 87.7 | 0.83 |
| | Object based | *Bhattacharya* | 59960.0 | 90.0 | 95.7 | 85.8 | 0.81 |

**Table 5.** Point based accuracy assessment of *Maxver* classifier error matrix using combined reference data ($N_3$ =219) across all land cover type classes.

| | **Class** | **Ground** | **Conifers** | **Deciduous** | ***H. pomanensis*** | **Column Total (CT)** | **Producer Accuracy (%)** |
|---|---|---|---|---|---|---|---|
| **Referencne data** | Ground | 56 | | 3 | 1 | 60 | 93.3 |
| | Conifers | | 27 | | 5 | 32 | 84.4 |
| | Deciduous | 5 | 2 | 67 | 2 | 76 | 88.2 |
| | *H. pomanensis* | 4 | | 5 | 42 | 51 | 82.4 |
| | Row Total (RT) | 65 | 29 | 75 | 50 | 219 | |
| User accuracy (%) | | 86.2 | 93.1 | 89.3 | 84 | **Overall accuracy (%)** | **87.7** |

*4.2 Point based accuracy assessment using error matrices.*

Results of the point based accuracy assessment using the combined reference data ($N_3$=219) showed that the *Maxver* classifier had user and producer accuracies greater than 82% across all land cover types (Table 5). The *Bhattacharya* classifier on the other hand had the highest producer accuracies (i.e. lowest omission errors) than the *Maxver* except for the deciduous trees land cover type (Table 6). Furthermore, the *Bhattacharya* classifier had user accuracies above 94% for all land cover type classes, except for the ground class, whereas the commission and omission errors of the *Maxver* classifier were similar across all land cover type classes (Table 6).

**Table 6:** Point based accuracy assessment of *Bhattacharya* classifier error matrix using combined reference data ($N_3$ =219) across all land cover type classes.

| | **Class** | **Ground** | **Conifers** | **Deciduous** | ***H. pomanensis*** | **Column Total** | **Producer Accuracy (%)** |
|---|---|---|---|---|---|---|---|
| **Reference data** | Ground | 56 | | 2 | | 58 | 96.6 |
| | Conifers | 1 | 35 | | 2 | 38 | 92.1 |
| | Deciduous | 21 | | 52 | | 73 | 71.2 |
| | *H. pomanensis* | 4 | | 1 | 45 | 50 | 90 |
| | Row Total | 82 | 35 | 55 | 47 | 219 | |
| User accuracy (%) | | 68.3 | 100 | 94.5 | 95.7 | **Overall accuracy (%)** | **85.8** |

*4.3. Hypothesis testing for point based accuracy assessment*

Statistical hypothesis testing was conducted to determine whether the $\hat{k}$ values of the two best performing classifiers i.e. *Maxver* and *Bhattacharya* in Table 4 were significantly different, hereafter denoted as $\hat{k}_M$ and $\hat{k}_B$, respectively. The results in Table 8 show the statistics used to calculate the standard normal deviate $Z_{MB}$ between $\hat{k}_M$ and $\hat{k}_B$. $Z_{MB}$ was calculated to be equal to 0.4983 (i.e. less than 1.96) therefore the null hypothesis that the *Maxver* classifier might not have given better classification results than the *Bhattacharya* classifier not rejected at the 95% confidence level.

**Table 7.** Statistics for the hypothesis test

| Classifier | $p_o\mathrm{X}$ | $p_c\mathrm{X}$ | $\hat{k}_\mathrm{X}$ | $\mathrm{var\_}\hat{k}_\mathrm{X}$ |
|---|---|---|---|---|
| *Maxver* | 0.8767 | 0.2727 | 0.8305 | 0.000871784 |
| *Bhattacharya* | 0.8584 | 0.2596 | 0.8088 | 0.001020260 |

Where $p_o\mathrm{X}$, $p_c\mathrm{X}$ and $\mathrm{var\_}\hat{k}_\mathrm{X}$ represent the overall accuracy, chance agreement and the variance of Kappa, respectively for image classifier X.

### *4.4. Comparison of Bhattacharya and Maxver Harrisia pomanensis areal estimates*

#### 4.4.1. Omission error areal estimates

Overall, the *Bhattacharya* classifier mapped very small *H. pomanensis* clumps with less omission error than the *Maxver* classifier with corresponding unmapped areal estimates of 9.3% and 37.8%, respectively (Table 8). While the pattern in mapping performance of the two classifiers across different area sizes of *Harrisia pomanensis* clumps is not clear, the results indicated that the *Bhattacharya* classifier gives the highest estimates of *H. pomanensis* for area sizes below 9 $m^2$ and between 12 and 21 $m^2$ compared to the *Maxver* classifier (Table 8). In addition, almost similar mapping performance by the *Bhattacharya* classifier was demonstrated for area sizes between 9 $m^2$ to 12 $m^2$ and 21 $m^2$ to 61 $m^2$ relative to the *Maxver* classifier (Table 8). These results suggest that the *Bhattacharya* classifier maps *Harrisia pomanensis* with the lowest omissions below 22% meanwhile the reported *Maxver* omission errors were up to approximately 40%.

**Table 8.** Mapping or detection areal estimates for the Maxver and Bhattacharya classifiers.

| | | | ***Maxver* classifier** | | ***Bhattacharya* classifier** | |
|---|---|---|---|---|---|---|
| Number of polygons (n) | Polygon size ($m^2$) | | Mapped area (%) | Unmapped area (%) | Mapped area (%) | Unmapped area (%) |
| 10 | Very small - Small | 0 - 9 | 62.2 | 37.8 | 90.7 | 9.3 |
| 8 | Small - Medium | 9 -12 | 60.7 | 39.3 | 84 | 16 |
| 8 | Medium - Large | 12 - 21 | 74.3 | 25.7 | 91.1 | 8.9 |
| 9 | Large – Verylarge | 21 - 61 | 63.6 | 36.4 | 78.4 | 21.6 |

#### 4.4.2. Demonstration of commission error occurrence for the *Maxver* and *Bhattacharya* classifiers using classification results.

The results shown in Figures 3-5 show extracts of the RGB UAV orthomosaic depicting *H.pomanensis* clumps digitized with a red polygon and subsequently how each classifier mapped the plant clump. This is to illustrate how each classifier omitted *H. pomanensis* pixels and mapped them as another class. The *Maxver* classifier has more mixed classes within the digitized polygons that the *Bhattacharya* classifier, and these qualitative area based accuracy results show the same pattern as point based accuracy assessment results in Tables 4-6.

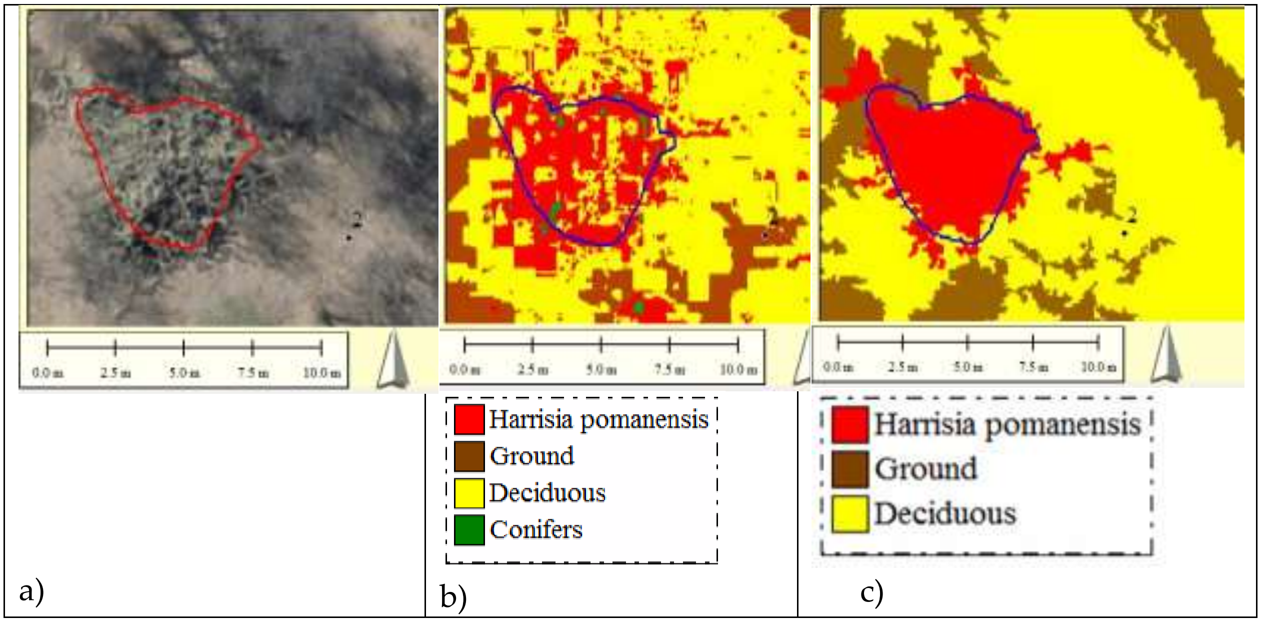


**Figure 3.** a) An extract of the UAV RGB image depicting a clump of *H. pomanensis* delineated by a visually interpreted 4.7 m$^2$ reference polygon in red, b) Selection of the *Maxver* classification map results for the same reference polygon and c) Selection of the *Bhattacharya* classification for the same reference polygon. In this scene there is no *H. pomanensis* plants far below (South) the polygon but the *Maxver* classifier (Figure 4b) committed a tree into the *H. pomanensis* class (red theme below the polygon).

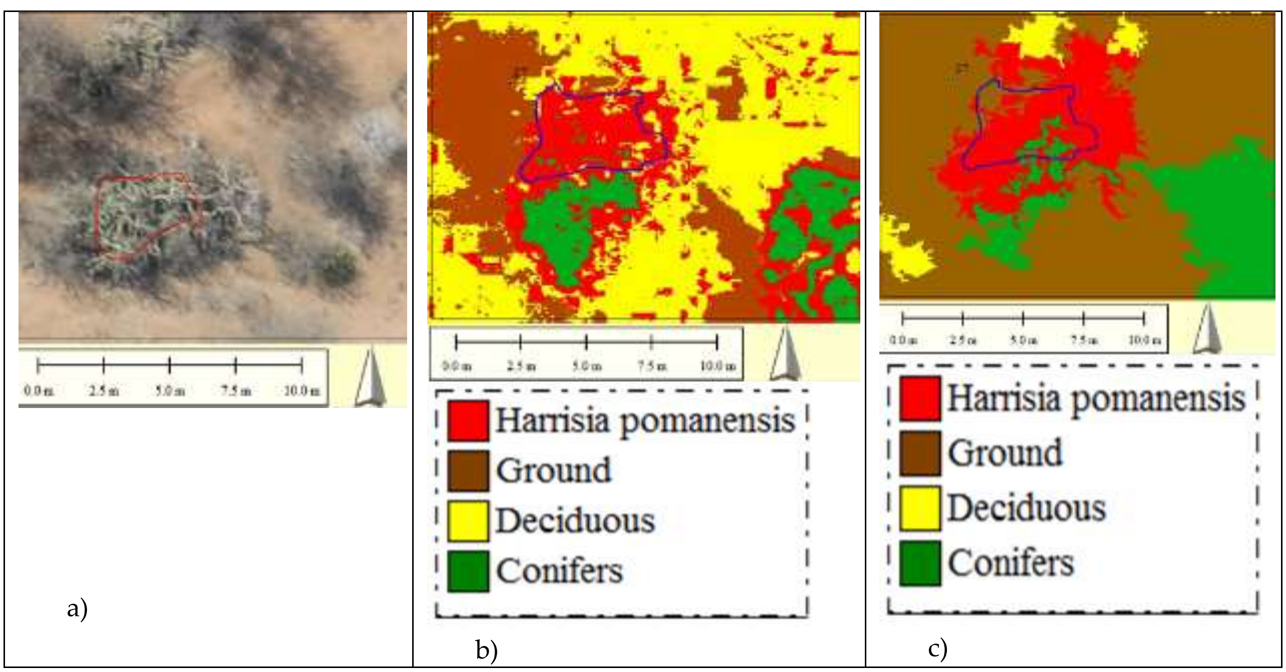


**Figure 4.** An extract of the 5 cm UAV RGB image depicting a clump of *H. pomanensis* delineated by a 22 m$^2$ visually interpreted reference polygon in red, b) Selection of the *Maxver* classification map results for the same reference polygon and c) Selection of the *Bhattacharya* classification for the same reference polygon. In this scene, there is not a significant amount of the *H. pomanensis* plant spikes outside the

polygon and therefore both *Maxver* classifier and *Bhattacharya* classifier committed other attributes into the *H. pomanensis* class. It seems that the *Bhattacharya* classifier committed more than the *Maxver* classifier in this scene immediately around the polygon. However, the *Bhattacharya* classifier detected the conifer (green theme) on the right bottom corner better than the *Maxver* classifier.

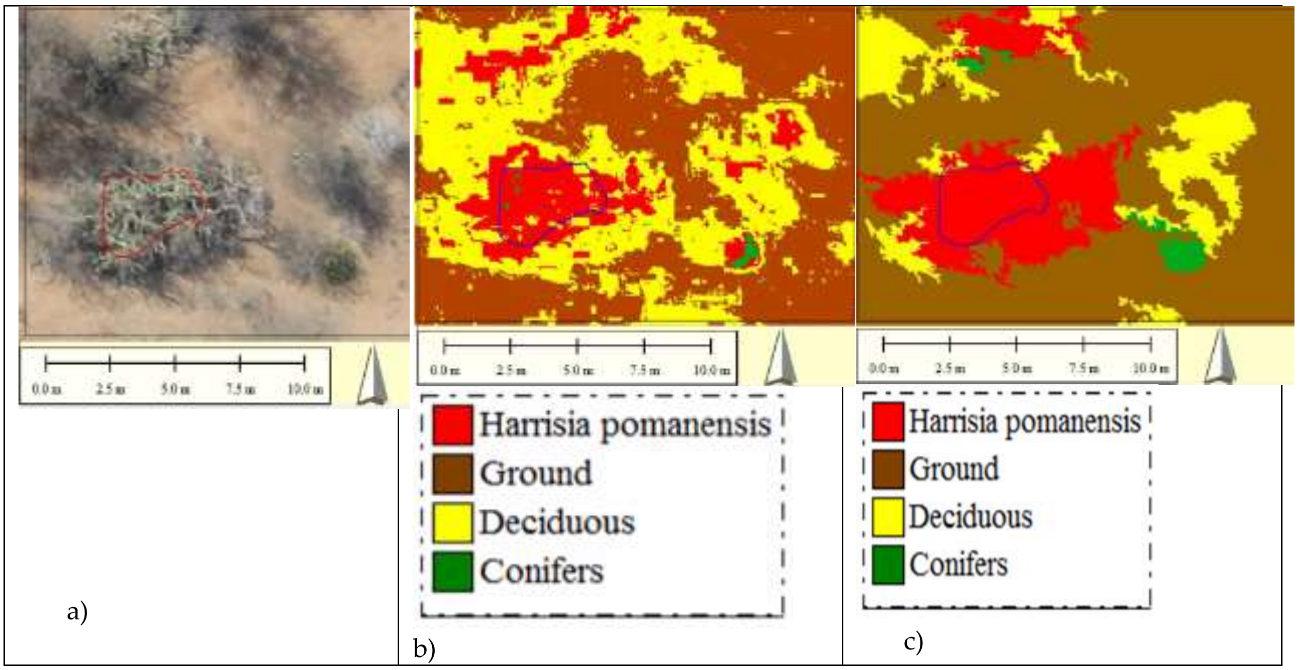


**Figure 5.** An extract of the 5 cm UAV RGB image depicting a clump of *H. pomanensis* delineated by a visually interpreted reference polygon in red, b) Selection of the *Maxver* classification map results for the same reference polygon and c) Selection of the *Bhattacharya* classification for the same reference polygon. On the far North side in this scene there is a clump of *H. pomanensis*. Both classifiers detected that clump but it seems that both of them overestimated its extent.

## 5. Discussion

This study evaluated five image classifiers for accurately mapping *Harrisia pomanensis* using two interlinked evaluation strategies (i.e. point and area based accuracy assessment) using a 3-band UAV derived RGB orthomosaic. The point based accuracy assessment results illustrated that the supervised image classifiers evaluated in this study generally produced better user and overall accuracies than the unsupervised classifiers for mapping *H. pomanensis*. The poor performance of the unsupervised image classifiers could be attributed to the low spectral resolution (approximately 100nm wide bands) of the utilized UAV imagery [53]. The evaluated unsupervised image classifiers depend only on the spectral resolution of the imagery because they make use of a linear comparison to assign a pixel/segment to a class according to a similarity measure that only takes into account a spectral mean or a median vector of the pixel/segment without taking into consideration textural and spatial information [41]. It is thus expected that for low spectral resolution UAV imagery, too many pixels/segments that belong to different land cover types will have similar spectral vectors and thus be classified together when they actually belong to different classes. This is explained by the generally low user and producer accuracies for the *K-mediuns, Euclidian length* and *Isoseg* classifiers. On the other hand, the supervised classifiers make use of probability models to assign pixels/segments to a class and that is why they outperformed their unsupervised counterparts for classifying low spectral resolution UAV imagery [53, 54]. In addition to the probabilistic models, supervised image classifiers make use of training data-sets to guide the classifier using not only single pixels/segments but a sample group of pixels/segments to train the classifier through machine learning [50].

Consequently, the use of error matrices based on the combined reference points ($N_3$ = 219) to compare the classifiers that were selected as the best performing classifiers (i.e. the supervised *Maxver* and *Bhattacharya* classifiers) was made in 4.2. On average, the object based *Bhattacharya* classifier gave higher producer and user accuracies than the pixel based *Maxver* classifier. However, the *Maxver* classifier gave a higher overall accuracy (87.7%) than the *Bhattacharya* classifier (85.8%) for the combined set of reference points ($N_3$ = 219). In addition to this, the *Maxve*r classifier produced a higher Kappa statistic estimate ($\hat{k}_M$=0.8305) than the Bhattacharya classifier ($\hat{k}_B$=0.8088) but the difference between these two kappa values was shown not be to be statistically significant at the 95% confidence interval in 4.3. To determine which algorithm works best for mapping *H. pomanensis*, use of the area based accuracy assessment was made. The area based accuracy assessment showed that the *Bhattacharya* classifier maps *H. pomanensis* better than the *Maxver* classifier with mapping averages of 86.1% and 65.2%, respectively. Additionally, the pixel based *Maxver* classifier produced thematic maps with the infamous salt and pepper effect. From these results we can deduce that the *H. pomanensis* spatial extent of 59960 $m^2$/872 000 $m^2$ (i.e. 6.9%) that is estimated by the *Bhattacharya* classifier with 90% and 95.7% producer and user accuracy for the combined reference points is more accurate than the spatial extents estimated by any other classifier in this evaluation (Table 4). The good *H. pomanensis* mapping accuracy by the *Bhattacharya* classifier is demonstrated in Figures 4-6. The Bhattacharya classifier is therefore recommended for mapping *H. pomanensis* under the current or similar environmental settings. These findings are in agreement with other studies because object based image analysis (OBIA) has been shown to be highly suitable for classifying very high spatial resolution but low spectral resolution UAV data than pixel based classification techniques [21]. ]. For instance, Laliberte et al., [57] obtained 86% overall accuracy ($\hat{k}$=0.81) for vegetation mapping in an arid rangeland plot using a supervised object based classification approach. The increased OBIA classification accuracy can partly be attributed to image segmentation algorithms such as the *region grown* technique used in this study because before image classification, segmentation creates objects that have a spatial or spectral homogeneity in one or more dimensions [58]. Moreover, it is possible to incorporate OBIA into the automation or semi-automation of remote sensing image classifiers [59]. We note that although image segmentation and classification algorithms can be improved for various application, other factors such as environmental conditions during the data acquisition need to be considered. For instance in this study, *H. pomanensis* was mapped in late winter in this study (13 August 2015) when the species is in a phenological stage that makes it different from the background woodland vegetation and when the deciduous trees are leafless this contributed to the success of OBIA. Moreover, OBIA was success full in mapping *H. pomanensis* as it takes into consideration spatial and textural information as *H. pomanensis* has both a different shape and texture compared to the other plants in the study area.

The UAV remote sensing sub-field is a promising approach for future mapping and detection of IAPs. This is because UAV remote sensing allows for mapping in inaccessible areas like the thorny woodland considered in this case study. Another advantage is that IAPs management practitioners in the future will likely have access to affordable integrated UAV and sensor systems than they do with traditional aircraft systems or satellite data [22]. Moreover, the high spatial resolution which can be attributed to the associated low UAV flight heights allows IAPs management practitioners to visually locate IAPs communities and clusters from true colour orthomosaics even before image classification. Advancements in battery technology, miniaturization of multispectral and hyperspectral sensors and design of more compact UAV and sensor systems all form a basis upon which better management, monitoring and eradication of IAPs will be possible in the future as spatial data is important for these IAPs management goals.

The limitation of this study is that *H. pomanensis* is sometimes found as an understory occurring invasive alien plant species. Thus all estimates based on aerial imagery might under estimate the true extent of *H. pomanensis* by not accounting for the clumps or stems that might be hiding underneath deciduous and coniferous trees. The problem of understory occurring invasive alien plant species has been frequently identified in remote sensing research [9, 17,12]. Remote Sensing methods for improving detection of understorey invasive alien plant species have been presented by [60-62]. An inherent limitation in the use of UAVs is the relatively small spatial extent when compared to airborne and satellite platforms. Additionally, low flight altitudes mean more images which may be labour intensive or require too much computing power for processing. When compared to traditional aerial surveying orthomosaics, UAV imagery orthorectification or georeferencing requires more GCPs and the surveying of GCPs is labour intensive.

## 6. Conclusions

The point-based accuracy assessment results showed that with reference to the combined set of reference points ($N_3$= 219), the supervised image classifiers mapped *Harrisia pomanensis* better than the unsupervised classifiers with user and producer accuracies of 82.4 % and 84% for the *Maxver* classifier as well as 90% and 95.7% for the *Bhattacharya* classifier. Even though the object-based *Bhattacharya* classifier gave higher user and producer accuracies than the pixel based *Maxver* classifier, the *Maxver* gave the highest overall accuracy of 87.7% and the highest Kappa estimate of 0.8305. A statistical hypothesis test was then conducted to test whether the *Maxver* Kappa estimate of 0.8305 was significantly greater than the *Bhattacharya* Kappa estimate of 0.8088 and we could not reject the null hypothesis that the two values are not statistically different at the 95% confidence interval. Additionally, the area based accuracy assessment results show that the *Bhattacharya* and *Maxver* classifiers estimated the spatial extent of *H. pomanensis* with an average detection accuracy of 86.1% and 65.2%, respectively. The area based accuracy assessment results also show that the *Bhattacharya* classifier was able to accurately map both small and large clumps of *H. pomanensis*. The Bhattacharya classifier is therefore recommended for mapping H. pomanensis under the current or similar environmental settings. These findings would be used to support the development of a semi-automated image classification system for mapping and monitoring *H. pomanensis*. The generic workflows in this scheme could be used for mapping other IAPs.

**Acknowledgments:** This research work was supported by the South African National Department of Environment Affairs through its funding of the South African National Biodiversity Institute Invasive Species Programme, project number P038. The authors would like to thank Dave Cochran, Phomolo Seriba, Owen Vyk and Malherbe Rossouw for assisting with the data acquisition process and provision of data processing equipment. Furthermore, the authors would like to thank Professor John R. Wilson and Kgatla Mahlatse for their insightful comments on the earlier version of this manuscript. We also thank Dr Helmuth Zimmermann for helping identify the woodland tree species. Last but not least, the authors would like to thank two anonymous reviewers for their helpful comments on this manuscript.

**Author Contributions:** M.M., P.T. and P.M. conceived the research idea. M.M. and P. T conducted the data analysis, literature review, tables, figures and preparation of manuscript. T. M and B. S. conducted the data acquisition and processing. J.B. and P. M. managed the preparation of the manuscript and performed editing.

**Conflicts of Interest:** The authors declare no conflict of interest.

## References


1. Pimentel, D.; Zuniga, R.; Morrison, Update on the environmental and economic costs associated with alien-invasive species in the United States. Ecol. Econ. **2005**, 52(3), 273-288.
2. Richardson, D. M.; van Wilgen, B. W. Invasive alien plants in South Africa: How well do we understand the ecological impacts? *S. Afri. J. Sci*.**2004**,100,45-52
3. Van Wilgen B. W. The evolution of fire and invasive alien plant management practices in fynbos. *S. Afri. J. Sci*. **2009**, 105, 9,335-342.
4. Vilà, M.; Espinar, J.L.; Hejda, M.; Hulme, P.E.; Jarošík, V.; Maron, J.L.; Pergl, J.; Schaffner, U.; Sun, Y.; Pyšek, P. (2011) Ecological impacts of invasive alien plants: a meta-analysis of their effects on species, communities and ecosystems. Ecol. Lett. **2011,** 14, 702-708.
5. Evangelista, P.H.; Stohlgren, T.J.; Morisette, J.T.; Kumar, S.Mapping invasive Tamarisk (Tamarix)—A comparison of single-scene and timeseries analyses of remotely sensed data. *Remote Sens*. **2009**, 1(3), 519–533.
6. Clout, M.N. & Williams, P.A. Invasive species management. A handbook of principles and techniques. Oxford University Press, Oxford, **2009**.
7. Wilson, J.R., Panetta, F.D. & Lindgren, C. Detecting and responding to alien plant incursions. Cambridge University Press, **2016**.
8. Wilson J.R.; Ivey P.; Manyama P.; Nanni I. (2013).A new national unit for invasive species detection, assessment and eradication planning. *S. Afri. J. Sci*. **2013**, 109, 5, 61-13.
9. Fox, J. C.; Buckley, Y. M.; Panetta, F. D.; Bourgoin, J.; Pullar, D. Surveillance protocols for management of invasive plants: modeling Chilean needle grass (*Nassella neesiana*) in Australia. *Diversity Distrib*. **2009**,12,577-589.
10. Müllerová, J.; Pergl J.; Pyšek, P. Remote sensing as a tool for monitoring plant invasions: Testing the effects of data resolution and image classification approach on the detection of a model plant species *Heracleum mantegazzianum* (giant hogweed).Int. J. Appl. Earth Obs. Geoinf. **2013**, 25, 55–65.
11. Underwood, E.; Ustin, S.; Di Pietro, D. Mapping non-native plants using hyperspectral imagery. *Remote Sens. Environ*. **2003**, 86, 150-161.
12. Huang, C.; Asner, G. P. Applications of remote sensing to alien invasive plant studies. *Sensors*.**2009,** 9, 4869-4889; doi:10.3390/s90604869
13. Ustin, S. L.; Santos M. J. Spectral identification of native and non-native plant species. *Proceedings of ASD and IEEE GRS; Art, Science and Applications of Reflectance Spectroscopy Symposium*. **2010**, 2, 1-17.
14. Williams, A. P.; Hunt, R. Estimation of Leafy spurge cover from hyperspectral imagery using mixture tuned matched filtering. *Remote Sens. Environ*. **2004**, 82(2), 446-456.

15. Agjee, N.; Mutanga, O.; Ismail, R.Remote sensing bio-control damage on aquatic invasive alien plant species. *South African Journal of Geomatics*, 2015, 4(4), 464-485
16. Ngubane, Z.; Odindi, J.; Mutanga, O.; Slotow, R. Assessment of the contribution of WorldView-2 strategically positioned bands in Bracken fern (Pteridium aquilinum (L.) Kuhn) mapping. *South African Journal of Geomatics*. **2013**, 3(2), 210-223.
17. Peerbhay, K.; Mutanga, O.; Ismail, R. The identification and remote detection of alien invasive plants in commercial forests: An overview. *South African Journal of Geomatics.***2016**, 5(1), 49-67.
18. Müllerová, J.; Pyšek, P.; JaroŠik, V.; Pergl, J. A. N. Aerial photographs as a tool for assessing the regional dynamics of the invasive plant species Heracleum mantegazzianum. *Journal of Applied Ecology*. **2005**, 42(6), 1042-1053.
19. Cochran, A. N. CIR imagery as a medium for mapping invasive alien vegetation' University of Johannesburg. Prepared for Working for Water (WFW), **2005**, 1-52.
20. Lucieer, A.; Robinson, S.; Turner, D.;Harwin, S.;Kelcey, J. Using a micro-UAV for ultra-high resolution multi-sensor observations of Antarctic moss beds. *Int. Arch. Photogramm. Remote Sens.* **2012,** XXXIX-B1, 429–433.
21. Laliberte, A.S.; Goforth, M.; Steele, C.M.; Rango, A.Multispectral remote sensing from unmanned aircraft: image processing workflows and applications for rangeland environments. Remote Sensing. **2011**, 3(11):2529-2551.
22. Dvořák, P.; Müllerová, J.; Bartaloš, T.; Brůna, J. Unmanned aerial vehicles for alien plant species detection and monitoring. **2015**, XL-1/W4, 83-139.
23. Wan, H.; Wang, Q.; Jiang, D.; Fu, J.; Yang, Y.; Liu, X.Monitoring the Invasion of Spartina alterniflora Using Very High Resolution Unmanned Aerial Vehicle Imagery in Beihai, Guangxi (China). The Scientific World Journal.2014: 1-7.
24. Müllerová, J.; Brůna, J.; Dvořák, P.; Bartaloš, T.; Vitkova, M;. Does the data resolution/origin matter? Satellite, airborne and UAV imagery to tackle plant invasions. *Int. Arch. Photogramm. Remote Sens.* **2016**,XLI-B7,XXIII:903-908.
25. Chen, G.; Zhao, K.; Powers, R. Assessment of the image misregistration effects on object-based change detection. *ISPRS Journal of Photogrammetry and Remote Sensing*. **2014**,87:19-27.
26. Pham, L.T.H.; Brabyn, L. Monitoring mangrove biomass change in Vietnam using SPOT images and an object-based approach combined with machine learning algorithms. *ISPRS Journal of Photogrammetry and Remote Sensing*. **2017**, 128:86-97.
27. Liu, Y.; Bian, L.; Meng, Y.; Wang, H.; Zhang, S.; Yang, Y. Shao, X.; Wang,B Discrepancy measures for selecting optimal combination of parameter values in object-based image analysis. *ISPRS Journal of Photogrammetry and Remote Sensing.* **2012**, 68: 144-156.
28. Hussain, M.; Chen, D.; Cheng, A.; Wei, H.; Stanley, D. Change detection from remotely sensed images: From pixel-based to object-based approaches. *ISPRS Journal*

*of Photogrammetry and Remote Sensing*. **2013**, 80: 91-106.
29. Sebari, I.; He, D. Automatic fuzzy object-based analysis of VHSR images for urban objects extraction. *ISPRS Journal of Photogrammetry and Remote Sensing*. **2013**, 79:171-184.
30. Camara, G.; Souza R. C. M.; Freitas, U. M.; Garrido, J.; SPRING: Integrating remote sensing and GIS by object-oriented data modelling. *Computers & Graphics*, **1996**, 20(3), 395-403.
31. Mzezwa, J.; Mlisi, T.; van Rensburg, L. Characterisation of rainfall at a semi-arid ecotope in the Limpopo province (South Africa) and its implications for sustainable crop production. *Water SA*, **2010**, 36(1), 19-26.
32. Schloderer, G.; Bingham, M.; Awange, J.L.; Fleming, K. M. Applications of GNSS-RTK derived topographical maps for rapid environmental monitoring: a case study of Jack Finney Lake (Perth, Australia). *Environ Monit Assess*, **2010**, 180(1-40,147-161.
33. Hedling, G.; Parker, A.; Wonnacott, R.TrigNet The Network of Active GPS Base Stations for South Africa. *Proceedings of the 13th International Technical Meeting of the Satellite Division of The Institute of Navigation (ION GPS 2000)*, **2000**, 1865-1870.
34. Chandler G. And Merry C. South African Geoid 2010: SAGEOID10. *Surveying Technical: PositionIT*. **2010**,29-33.
35. Gini, R.; Pagliari, D.; Passoni, D.; Pinto L.; Sona, G.; Dosso, P. UAV photogrammetry: Block Triangulation Comparisons. *ISPRS - Archives*, **2013**, XL-1/W2, 157-162.
36. Gallaun, H.; Steinegger, M.; Wack, L.; Schard, M.; Kornberger, B.; Schmitt, U. Remote Sensing Based Two-Stage Sampling for Accuracy Assessment and Area Estimation of Land Cover Changes. Remote Sens. **2015**, 7(9), 11992-12008.
37. ESRI, ArcGIS A Complete Integrated System. Environmental Systems Research Institute,Inc.,Redlands,California.Availableonline:http://www.esri.com/software/arcgis/arcgis-for-desktop (Accessed on 17 February **2016**).
38. Osborne, M. Arduplot Mission planner. Available online: http://planner.ardupilot.com/ (Accessed on 10 August **2015**).
39. Agisoft LLC. Agisoft PhotoScan. Available online: http://www.agisoft.com/downloads/installer/ (Accessed on 15th June 2015).
40. Wang, Q.; Wu, L.; Chen, S.; Shu, D.; Xu, Z.; Li F.; Wang, R. Accuracy evaluation of 3D geometry from low-attitude UAV images: A case study at Zijin mine. *ISPRS – Archives*. **2014**, XL-4, 297-300.
41. Wang, L.; Zhang, Y.; Feng, J. On the euclidean distance of images. *IEEE Transactions on Pattern Analysis and Machine Intelligence*. **2005**, 27(8), 1334–1339.
42. Yang C., Everitt J. H. And Murden, D. Evaluating high resolution STOP 5 satellite imagery for crop identification. *Computers and Electronics in Agriculture, Netherlands*. **2011,** 75,347-354.

43. Silva, A. F.; Barbosa, P. A.; Zimback, C. R. L.; Landim P. M. B. Geostatistics and remote sensing methods in the classification of images of areas cultivated with citrus'. Engineering Agriculture.**2013**, 33(6), 1245-1256.
44. Blaschke, T.; Strobl, J. What's wrong with pixels? Some recent developments interfacing remote sensing and GIS. *Geo-Informations-Systeme*. **2001**, 14(6), 12-17.
45. De Maesschalck, R.; Jouan-Rimbaud, D.; Massart, D. L. The Mahalanobis distance. *Chemometrics and Intelligent Laboratory Systems***.** **2000**, 50, 1-18.
46. Duda, R. O.; Hart P. E. Pattern Classification and Scene Analysis. John Wiley and Sons, New York, USA,**1973**
47. Filho, R. A., Vitorello I. and Bins L. S. A (1997). Application of image merging, segmentation and region-classification techniques as a new approach for the detailed thematic mapping of soil-vegetation assemblages. *Revista Brasileira de Geociências* **1997**, 27(2), 203-206.
48. Choi, E.; Lee, C. Feature extraction based on the Bhattacharyya distance. *Pattern Recognition* **2003**, 36, 1703-1709.
49. Lentilucci, E.J. On using and computing the Kappa statistic, Tech. Rep. Rochester Institute of Technology, College of Science, Center for Imaging Science, Digital Imaging and Remote Sensing Laboratory, Rochester, New York, United States, **2006**.
50. Senseman, G. M.; Bagley, C. F.; Tweddale, S. A. Accuracy assessment of the discrete classification of remotely-sensed digital data for land-cover mapping. USACERL Technical Report EN-95/04. U. S. Army Corps of Engineers, Champaign,IL, **1995**, 1-27.
51. Congalton, R. G. A review of assessing the accuracy of classifications of remotely sensed data. Remote Sens. Environ **1991**, 37, 35-46.
52. Congalton R. G.; Oderwald, R. G.; Mead R. A. Assessing Landsat classification using discrete multivariate statistical techniques. *Photogramm. Eng. Remote Sens*. **1983**, 46(12), 1671-1678.
53. Müllerová, J.; Brůna, J.; Dvořák, P.; Bartaloš, T.; Vítková, M. Does the data resolution/origin matter? Satellite, airborne and UAV imagery to tacle plant invasions. The International Archives of the Photogrammetry, Remote Sensing and Spatial Information Sciences, **2016**, XLI-B7, 903-908
54. Wang, L.; Zhang, S. Incorporating of texture information in a SVM method for classifying Saltcedar in Western China. *Remote Sens. Lett.* **2014**, 5(6), 501-510.
55. MacLean, M. G.; Congalton, R. G. Investigating issues in map accuracy when using an object-based approach to map benthic habitats. GIScience and Remote Sensing, **2011**, 48(4), 457-477.
56. Lary, D.J.; Alavi A. H.; Gandomi, A. H.; Walker A. L. Machine learning in geosciences and remote sensing. Geoscience Frontiers, **2016**, 7, 3-10.

57. Laliberte, A. S. Image processing and classification procedures for analysis of sub-decimeter imagery acquired with an Unmanned Aircraft over arid rangelands. GIScience and Remote Sensing. **2011**, 48(1):4-23.
58. Blaschke, T. Object based image analysis for remote sensing. *ISPRS Journal of Photogrammetry and Remote Sensing*. **2010**,65:2-16.
59. Benz, C.; Hofmann, P.; Willhauck, G.; Lingenfelder, I.; Heynen, M. Multiresolution, object-oriented fuzzy analysis of remote sensing data for GIS-ready information. *ISPRS Journal of Photogrammetry and Remote Sensing*. **2004**, 58: 239-258
60. Joshi, C.; De Leeuw, J.; van Andel, J.; Skidmore, A. K.; Lekhak, H. D.; van Duren, I.C; Norbu, N. Indirect remote sensing of a cryptic forest understorey invasive species. Forest ecology and management. **2006**, 225(1-3), 245-256.
61. Wang, T.; Skidmore, A.; Toxopeus, A. Improved understorey bamboo cover mapping using a novel hybrid neural network and expert system. *Int. J. Remote Sens*.**2009**, 30(4), 965-981.
62. Tuanmu, M.; Vina, A., Bearer, S., Xu, W., Ouyang, Z., Zhang, H., Liu, J. Mapping understory vegetation using phenological characteristics derived from remotely sensed data. *Remote Sens. Environ*, **2010**, 114, 1833-1844.